DOI: 10.1111/cgf.15040
EUROGRAPHICS 2024 / A. Bermano and E. Kalogerakis
(Guest Editors)

COMPUTER GRAPHICS *forum*
Volume 43 (2024), Number 2

3D Reconstruction and Semantic Modeling of Eyelashes

G. Kerbiriou[1,2], Q. Avril[2] and M. Marchal[1,3]

[1]Univ. Rennes, INSA, IRISA, France
[2] InterDigital, France
[3] IUF, France

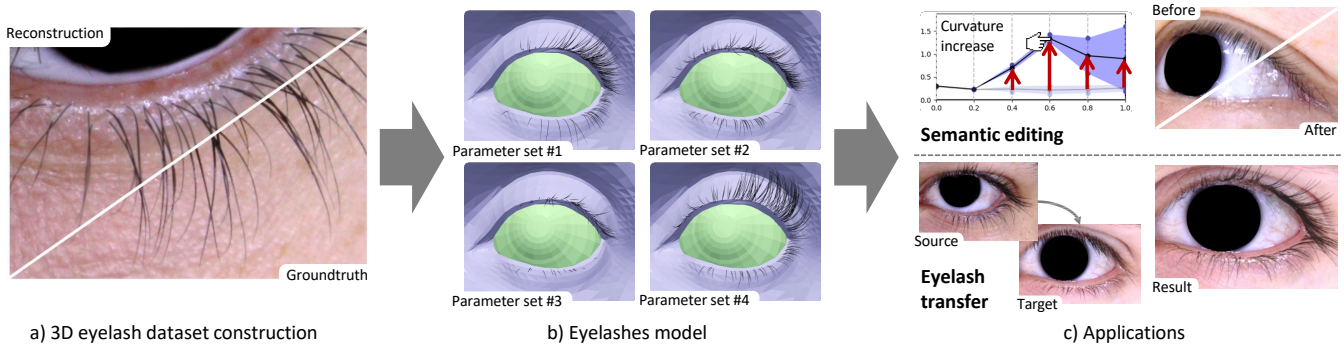

Figure 1: *Overview of our pipeline. (a) 3D eyelashes are reconstructed using a novel approach from a multi-view ocular region dataset (Section 3). (b) Our semantic eyelashes model is calibrated based on real data (Section 4) and (c) can be used for various applications such as eyelash semantic editing or eyelash transfer (Section 5).*

Abstract

High-fidelity digital human modeling has become crucial in various applications, including gaming, visual effects and virtual reality. Despite the significant impact of eyelashes on facial aesthetics, their reconstruction and modeling have been largely unexplored. In this paper, we introduce the first data-driven generative model of eyelashes based on semantic features. This model is derived from real data by introducing a new 3D eyelash reconstruction method based on multi-view images. The reconstructed data is made available which constitutes the first dataset of 3D eyelashes ever published. Through an innovative extraction process, we determine the features of any set of eyelashes, and present detailed descriptive statistics of human eyelashes shapes. The proposed eyelashes model, which exclusively relies on semantic parameters, effectively captures the appearance of a set of eyelashes. Results show that the proposed model enables interactive, intuitive and realistic eyelashes modeling for non-experts, enriching avatar creation and synthetic data generation pipelines.

CCS Concepts

• ***Modeling/Geometry*** → *Facial Modeling; Datasets/Evaluation/Perception; Hair Modeling;*

1. Introduction

For several decades, digital human creation, animation and rendering have received considerable attention from the computer graphics community. Realistic virtual avatars are now a key aspect of our digital life such as in virtual reality, visual effects, gaming and advertising. The complexity of the human face has led researchers to adopt a specialization strategy for the different anatomical components of the face in order to tackle the global shape and appearance of the head [BV99; LBB*17; GTZN21], neck [LZX*21], jaw [YMS*19], tongue [PMTZ22], teeth [WBG*16; VPB*18], ears [DPS18], scalp hair [NWKS19; ZHX*18; CSW*16; WNS*22] or facial hair [BBN*12; LJZ*23; LHWD17] independently. From a perception point of view, the ocular region is one of the most important facial elements [RWX17; KPKR17; BWH*01] to have also received an important focus, especially on eyeballs [BBN*14; BBGB16; BBGB19; WBM*16a; SWW*20] and eyelids [BBK*15; NCRP16; KADM22]. But so far, eyelashes have rarely been studied and modeled despite playing a critical role in the aesthetics and expressiveness of the human face. Their intricate arrangement around the eye not only serves functional purposes, such as protecting the

eyes from foreign particles, but also significanlty contributes to the overall appearance and attractiveness of an individual [Ada21]. As a result, the subtle nuances of eyelashes in their distribution, length, orientation, curvature or even thickness require specialized attention in the context of digital human face modeling.

The particularity of eyelashes does not only lie in their critical location. Eyelashes are distinct from scalp and body hair. They are notably shorter and finer in texture, and can be seen as one-dimensional fibers. Upper eyelashes curve upward and away from the eye, while lower eyelashes point downward. Due to their very specific characteristics and their central role in facial appearance, modeling digital eyelashes represents a key challenge in computer graphics for designing a wide variety of eyes.

Despite the impact of eyelash aesthetics, 3D artists do not yet have access to dedicated eyelashes creation tools. Instead, they work with generic hair creation modules embedded in 3D software [Fou23; Aut23; Sof23; Max23b; Max23a]. The typical workflow is to instantiate a set of guide curves (or ribbons or meshes) to roughly define the eyelash shapes. First, artists position the anchor (root) of each guide curve and proceed to give them an adequate appearance. To do so, current tools propose shape operations such as cutting, twisting, noising, curling and many others. This 3D modeling workflow offers a lot of freedom, but obtaining the desired eyelashes is far from being accessible to non-experts.

In video-games and real-time applications, eyelashes are often rendered using transparent textures mapped onto polygonal strips that follow the eyelid ridges, thus offering small memory consumption and rendering time cost. In return, they are impossible to edit unless recreated from scratch. As a remedy, character-creation solutions [Rea22; Com20; Gam23] and synthetic data-generation methods [WBM*16b; WBH*21; XZZ*21; WNS*22] usually rely on banks of handcrafted eyelashes. However, this solution requires a lot of careful work from artists and severely limits the diversity of the samples generated.

In this work, we introduce the first semantic data-driven model of eyelashes together with an original 3D reconstruction methodology. It addresses an interesting gap in existing research for eyelash design, thus proposing novel directions in the digital human creation. Unlike former approaches, our model harnesses the power of data not only to capture the intricate complexities of eyelash morphology but also to deliver high realism and flexibility. In the spirit of existing face models, our data-driven eyelashes model enables artists and animators to create lifelike digital eyes, thus enhancing immersion and storytelling in virtual worlds. Moreover, this innovation extends beyond entertainment, finding practical applications in industries such as cosmetics, virtual try-on, and medical simulations, where realistic eyelash representation is paramount. Researchers today often resort to manual annotation of photographs or invasive *in vivo* procedures to study eyelash properties, which makes the process time-consuming, labor-intensive, and ethically challenging. By offering a fully automatic and non-invasive 3D eyelash reconstruction solution, we open new avenues for understanding and collecting eyelash data in medical research.

Our contributions, summarized in Figure 1, are the following:

- A novel approach for high-quality 3D eyelashes reconstruction.
- The first publicly available dataset of 3D eyelashes containing a total of 57 subjects.
- A semantic data-driven model of eyelashes based on spatial distributions of eyelash aesthetics.
- Various applications of our model including eyelashes resampling, eyelashes transfer and interactive semantic eyelashes editing.

The paper is organized as follows: first, Section 2 reviews the state-of-the-art around the 3D reconstruction and modeling of eyelashes. Then, Section 3 introduces the creation of the eyelashes dataset through our novel 3D eyelashes reconstruction methodology. Section 4 presents the novel eyelashes model, including parameter estimation based on real data. We demonstrate our approach on a wide variety of results in Section 5. Finally, Section 6 and Section 7 conclude the paper and discuss future work.

2. Related Work

The 3D reconstruction and modeling of eyelashes requires to characterize, reconstruct and model them. The state-of-the-art of these topics are presented in the following paragraphs.

Eyelash characterization has been specifically studied for medical and cosmetic design research. Na *et al.* [NKK*06] compared the eyelashes of Caucasian and Asian women on several physical properties such as length, degree of curvature and density obtained via manual image annotation. Spatial information is obtained by discretizing the eyelid into five uniform regions. Similarly, Kikuchi *et al.* [KMI*15] measured the length, density, curvature and root lift (elevation) angle in Japanese female individuals from frontal and lateral photographs. They set up an *ad-hoc* threshold to decide whether an eyelash is curved or straight. Shaiek *et al.* [SFF*18] used dedicated software to count the upper eyelashes on photographs and extract geometrical features in view of mascara assessment, but they did not provide any implementation details. In another setting, Tohmyoh *et al.* [TIIW18] studied the internal physical properties of eyelashes and their correlation with the observable curvature. The studies listed have brought new insights into eyelash characterization, but they do not rely on accurately reconstructed 3D eyelashes, which could make it possible to gather more qualitative and quantitative data. 3D reconstruction of eyelashes may come close to other facial elements such as hair and facial hair.

Scalp hair 3D reconstruction has been extensively studied in the past two decades. Existing methods typically rely on dense vector fields extracted from images combined with photometric and geometric constraints, often followed by a bottom up hair growing strategy [PBS04; PCK*08; LLP*12; LLR13; WOQS05; NWKS19]. To enhance reconstruction fidelity, researchers leveraged various sensor modalities including depth-of-focus devices [JMM09], thermal imaging [LWZ12], RGB-D cameras [HML*14] and Computed Tomography [SSW*23]. Nam *et al.* [NWKS19] proposed a line-based multi-view stereo algorithm with a new objective function, but their solution relies on a dense setup of 70 cameras. Based on this, Sun *et al.* [MSN*21] incorporated a parametric hair reflectance model and light code system to improve the results

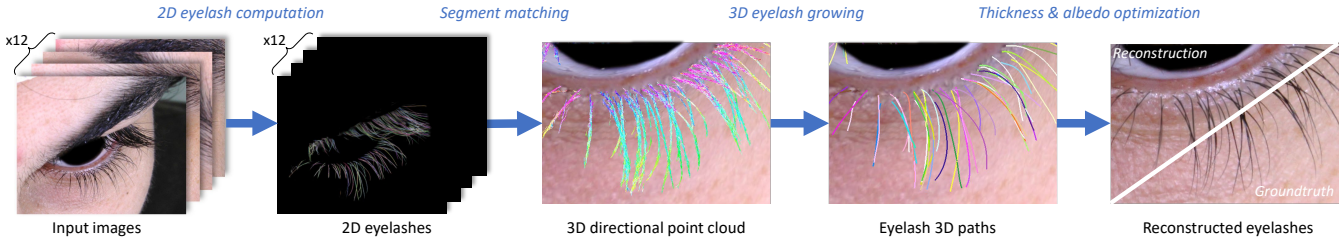

Figure 2: *Overview of our eyelash reconstruction pipeline. It is composed of a 2D eyelash computation step (Section 3.3), a multi-view stereo segment matching stage (Section 3.4), a 3D eyelash growing phase (Section 3.5) and a thickness and albedo estimation process (Section 3.6).*

in an inverse rendering scheme with 24 views. When they reduced the number of cameras needed, they only used synthetic data to evaluate their method. Rosu *et al.* [RSW*22] learnt a generative strand-based hair model tailored for differentiable neural rendering, which offered photo-realistic view dependent results and fine strand editing. Following this idea, Sklyarova *et al.* [SCD*23] used the Soft Rasterization framework [LLCL19] as a differentiable rasterizer, arguing that the gradients computed from multiple hair layers led to improved results. However, the above approaches require a heavy setup with controlled lighting or consequent prior model learning. The need for such complex systems can be explained by the heavily occluded nature of scalp hair, a characteristic not shared with facial hair such as eyelashes.

Facial hair 3D reconstruction has been subject to less research than scalp hair modeling, but several approaches have already laid important foundations in the field. In particular, Beeler *et al.* [BBN*12] proposed to perform a coupled reconstruction of skin and sparse facial hair from a passive setup of 14 cameras and uniform lighting. They presented a bottom-up approach where 2D line segments were extracted from orientation fields, using a hair growing strategy. 3D hairs were then matched from view pairs and accurately reconstructed with additional filtering steps. Years later, this method was exploited for facial hair tracking [WZC*22]. In the same vein, Fyffe [Fyf12] investigated advanced image processing techniques to extract 3D facial hair from six views. The result however is an unstructured point cloud. These methods can effectively recover facial hair geometry, but the reconstruction quality is not satisfactory in the ocular region. Moreover, they require the manual cleaning of numerous false positives. Their main flaw resides in the 2D hair detection step which relies on hand-crafted image processing algorithms that particularly struggle to detect eyelashes. Rotger *et al.* [RMLA19] formulated a solution for the challenging case of single-view facial hair reconstruction. While their method outputs visually correct results, the reconstruction quality does not match multi-view methods. None of the above-mentioned work has specifically addressed the reconstruction of eyelashes, by taking into account their remarkable implantation pattern, for instance. Eyelash-specific features must be well understood for their reconstruction as well as for their representation in a model.

3D fibers representation and modeling. Various 3D fibers representations such as node sequences [BBN*12; NWKS19] or point clouds [Fyf12] have been proposed for modeling 3D fibers. Physics-oriented models such as piecewise helices [BAC*06; RMLA19], discrete elastic rods [BWR*08], or more recently, latent code representations [WNS*22] have also been proposed.
In the context of facial hair, Herrera *et al.* [LZWV10] built a statistical model of facial hair based on registered scan textures. They extracted *ad-hoc* features in the image domain that are used to generate a hair probability density map. Synthesizing facial hairs then consists in sampling pixel positions with this map from which filaments are grown using an orientation map. Legendre *et al.* [LHWD17] modeled the vellus hair from backlit images of a subject by computing image statistics and determining the parameters of a dedicated hair model that best fit the observations. Very recently, Li *et al.* [LJZ*23] attempted 3D eyebrows modeling from a single image. After the creation by artists of a large dataset of synthetic eyebrows based on real images, they trained three neural networks that operate on an input image to respectively predict the root position, orientation and length of eyebrow hair. All the listed methods succeeded in extracting information about a specific type of hair, but they did not enable semantic control. In contrast, and concerning eyelashes, introductory work by Sacha *et al.* [SFWV06] presented the first profile-based statistical model of eyelashes. Each individual eyelash is represented as a three-point model parameterized by its length, orientation, curvature and thickness. Distributions of these parameters along the eyelid path or eyelash length are then materialized using profile curves, thus enabling intuitive semantic editing. However, their model is not data-driven and does not guarantee the generation of anatomically realistic eyelashes. It also omits important parameters such as density and albedo. In addition, their eyelash model is defined with respect to a global reference frame which makes head transformation and eye reposing impractical.

Conclusion. While the literature includes methods that could be used to collect 3D eyelash data, they can be improved by taking into account eyelash specificities such as their implantation, length and monotonous curvature. In the same way, there are no eyelashes models that enable intuitive semantic editing while ensuring anatomically realistic results. In this paper, we aim to tackle these specific limitations of the current state-of-the-art. For that purpose, we designed a reconstruction method that is specific to eyelashes, and employed it to recover the eyelash geometry from an eye region multi-view dataset. The unique resulting data is leveraged to calibrate a generative eyelashes model where the aesthetic of each individual eyelash is described using few semantic parameters such as length, curvature and uplift angle. Altogether, these methods for 3D reconstruction and modeling are applied to several applications

such as eyelash resampling, eyelash transfer and interactive semantic eyelash editing.

3. 3D Eyelash Reconstruction

3.1. Overview

To capture all the specificities of the eyelashes and calibrated our associate model, we built an original 3D eyelashes dataset. To do so, we developed a state-of-the-art 3D reconstruction method that is specific to eyelashes, and used it to recover the eyelash geometry and appearance from an existing eye region multi-view dataset [KADM22]. Figure 2 shows an overview of our dataset construction methodology. First, we use EyelashNet [XZZ*21] to perform precise eyelash segmentation. EyelashNet is a Convolutional Neural Network tailored for this specific task. Figure 4 shows an example of an image of an eye and its segmentation. Subsequently, these segmented eyelash regions are input into a specialized 2D eyelash growth and filtering algorithm. The resulting two-dimensional eyelash structures serve as input for a multi-view stereo segment matching algorithm, which enables the generation of a three-dimensional point cloud where each point is associated with the eyelash growth direction. Using this directional point cloud, the algorithm synthesizes and refines 3D eyelashes, by employing a filtering process to ensure accuracy and realism in the reconstructed geometry. Finally, we optimize eyelash thickness and albedo in an inverse rendering process that takes into account depth-of-field blur. This comprehensive approach offers a robust solution for achieving high-fidelity 3D eyelash reconstruction based on multiple images. The next paragraphs detail each step of our 3D reconstruction approach.

3.2. Eyes Dataset

We leveraged the dataset of posed eyes built by Kerbiriou *et al.* [KADM22], which contains more than $2k$ eye region scans among 57 volunteers (41 males and 16 females from 21 to 67 years old). Each eye region is reconstructed using photogrammetry from 12 views, and registered with a template mesh, as depicted in Figure 3. For each volunteer, 36 eye poses (9 different gaze angles combined with 4 different eye apertures) are reconstructed , thus allowing for geometrically accurate rigging by tri-linear interpolation (horizontal gaze angle, vertical gaze angle and eye aperture). In this work, only the neutral eye pose is considered, which corresponds to forward gaze and a normally open eye. The neutral pose indeed contains enough information about eyelashes since they move rigidly with their attachment point due to their small length. Both images and 3D information are used to reconstruct the eyelashes. For data security and privacy considerations, the irises of the eyes sourced from this dataset have been masked in this paper. However, the computations were performed without masks.

3.3. 2D Eyelash Growing

Once the data segmentation has been performed, we grow 2D hairs in each image as depicted in Figure 4. In an initial step, we follow the 2D hair reconstruction method proposed by Beeler *et al.* [BBN*12], but we input the EyelashNet segmentation

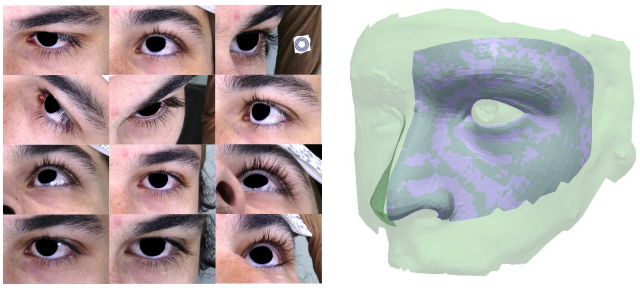

Figure 3: *A data sample from Kerbiriou et al. [KADM22]: (Left) The twelve views of a volunteer's left eye and (Right) the reconstructed and registered surfaces in green and blue, respectively.*

[XZZ*21] instead of the *hair map*. The *hair map* was obtained with orientation filtering and a parameter ν that manages the hair detection tolerance. Replacing the *hair map* with EyelashNet's segmentation guarantees much higher precision, a lower rate of false positives, and makes it possible to bypass the need for the parameter ν.

The 2D eyelashes, which are represented as sequences of 2D segments, are iteratively grown by searching for the most coherent growing direction in the eyelash segmentation map using a cone shaped filter. Since eyelashes are particularly straight compared to beard hair, we got better results with a narrower cone than the one in the original paper, with $\gamma = 36$ degrees instead of $\gamma = 60$ degrees. In practice, we want to generate as many 2D segments as possible in the flow of eyelashes in order to generate the densest 3D directional point cloud possible later on. To do so, we used the previous algorithm twice, once with rejection sampling which means that a new seed cannot be located too close (10 pixels) to an existing 2D eyelash, and once without. This makes it possible to obtain over 1000 2D eyelashes. A part of them happens to be misaligned because of occluded eyelashes which results in abnormally thick segmentation. We computed the angle difference of each eyelash with the orientation map, and discarded those with an average angle difference that exceeds a certain threshold. The orientation map is obtained by filtering the segmentation map with Gabor kernels. In our experiments, we identified an optimal threshold value of 40°. When using lower values, good quality eyelashes are discarded, while higher values tend to retain some visually misaligned hairs. Figure 4 shows a qualitative result of the filtering step in a challenging area.

3.4. 3D Eyelash Segments Matching

In the baseline method of Beeler *et al.* [BBN*12], the whole *2D hairs* are matched in 3D, resulting in a set of piecewise linear chains of 3D hair segments. In contrast, we directly match the *2D segments* to form 3D segments, and we again use EyelashNet's segmentation instead of the *hair map* in the *matching matrix*, but the core matching algorithm remains unchanged. For a detailed description, the reader may refer to the original paper.

Compared to the set of 3D hair pieces in the original method,

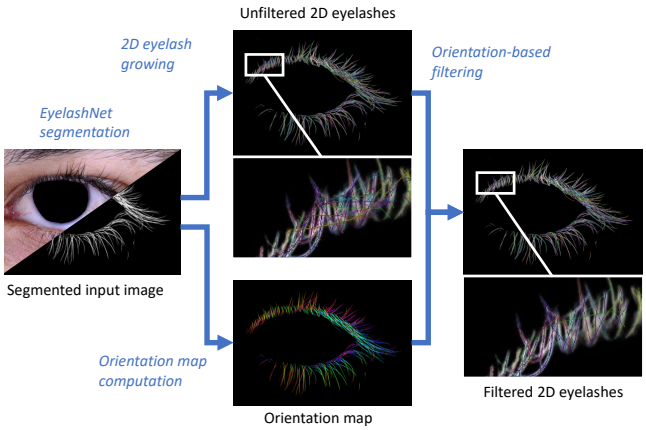

Figure 4: *2D eyelashes computation pipeline. The orientation based eyelash filtering removes the major part of misdirected hairs.*

our directional point cloud is easier to filter in the case of 3D eyelashes reconstruction. The directional point cloud is filtered by a confidence measure for each point. We defined a score of affinity α between two directed points $P_i = \{\mathbf{p_i}, \mathbf{d_i}\}$ and $P_j = \{\mathbf{p_j}, \mathbf{d_j}\}$ as a product of three cosines:

$$\alpha(P_i, P_j) = |\mathbf{d_i} \cdot \mathbf{d_j}| \cdot |\mathbf{d_i} \cdot \frac{\mathbf{p_j} - \mathbf{p_i}}{||\mathbf{p_j} - \mathbf{p_i}||}| \cdot |\mathbf{d_j} \cdot \frac{\mathbf{p_j} - \mathbf{p_i}}{||\mathbf{p_j} - \mathbf{p_i}||}| \quad (1)$$

The affinity score is close to one when the two points share a similar direction and are well aligned. One advantage of this metric is that it is scale-agnostic. For each point, confidence score $\overline{\alpha}$ is computed as the averaged affinity score of its k neighbors:

$$\overline{\alpha}(P_i) = \sum_{P_j \in k\text{-neighs}(P_i)} \frac{\alpha(P_i, P_j)}{k} \quad (2)$$

The goal of this metric is to identify if the points have enough neighbors that share a good affinity score, in which case they are likely to be valid points. In our experiments, we used $k = 150$. A smaller value of k produces over-localized confidence while a greater one can make it possible to compute the confidence level with points from other eyelashes. The confidence score appears to be a great indicator of false positives. Removing all the points with a confidence score lower than 0.2 greatly improves the sharpness of the point cloud without losing too much point density (Figure 5).

3.5. 3D Eyelash Growing

Similar to 2D eyelash growing, 3D eyelashes are grown using a bottom-up approach where the base material is the directional point cloud obtained via multi-view stereo. The reconstructed eyelashes are in the form of a list of directed points $\{P_0, ...P_i, ...P_N\}$. We select the directed point with the greatest confidence score and start searching for the next point in the two directions given by its orientation. Points outside a closed cone of length $l = 0.7$mm with

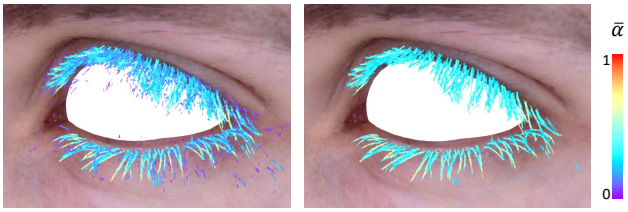

Figure 5: *Visualization of the directional point cloud obtained via multi-view stereo (confidence score in false colors). Left: all directed points, right: only points with a confidence level greater than* 0.2.

an aperture of 13.5°oriented in one of the given directions are discarded. The cone is narrower than in the original method (40 °) [BBN*12] since eyelashes are particularly straight compared to other facial hair. The next point is computed by blending the candidate points C into a weighted average. The weights are their affinity score relative to the current point:

$$\mathbf{p}_{i+1} = \frac{\sum_{P_j \in C} \alpha(P_i, P_j) \cdot \mathbf{p}_j}{\sum_{P_j \in C} \alpha(P_i, P_j)}, \ \mathbf{d}_{i+1} = \frac{\sum_{P_j \in C} \alpha(P_i, P_j) \cdot \mathbf{d}_j}{\sum_{P_j \in C} \alpha(P_i, P_j)} \quad (3)$$

The start point is removed from the directional point cloud, and so are the candidate points. This process is repeated for both ends while there are at least 3 points in the current candidate point set. Next, the new point with the highest averaged α is selected as a seed. We use rejection sampling and discard any seed that is closer than 0.2 mm to any other eyelash. The 3D hair growing algorithm eventually stops when the directional point cloud is empty.

The resulting reconstruction is usually exhaustive but many eyelashes are invalid: some are too short, some are rooted too far from the skin and some are duplicates (Figure 6). To solve this issue, we perform a filtering process in several steps. First we remove the eyelashes measuring less than 2 mm and those which are more than 8 mm away from the eyelid edges. Next, we continue to grow each eyelash using the segmentation maps instead of the directional point cloud. Specifically, for each 3D eyelash end, we generate an array of candidate points in front of the last point, following the direction of the last segment. We connect each candidate point to the end point, project the resulting segment onto each of the 12 views, and calculate the average pixel value it covers on the segmentation maps. If the highest average value is greater than 0.4, we grow the eyelash with the corresponding candidate point. Finally, when two hairs are closer than 0.1 mm on average, the shortest one is removed. These values, empirically chosen, lead to good results for most data samples. Figure 6 shows a qualitative result of this filtering process.

3.6. Eyelash Thickness and Albedo Estimation

To obtain more precise reconstruction, we further investigated the estimation of the thickness and albedo (diffuse color) of the eyelashes. We observed that the depth-of-field blur in the images makes the eyelashes appear slightly thicker than they really are.

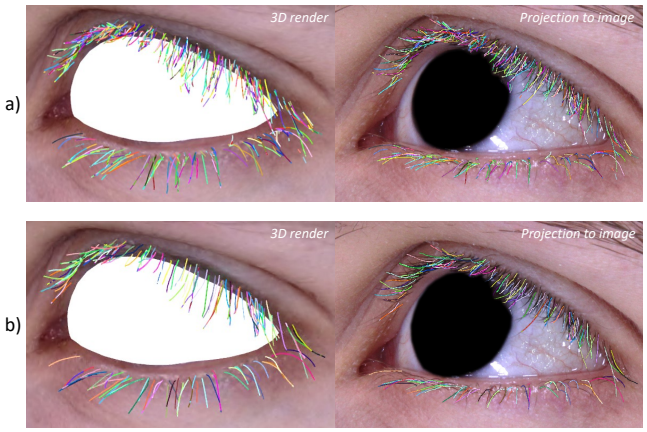

Figure 6: *Raw 3D eyelashes (a) right after the 3D hair-growing algorithm and after the filtering steps (b). Notice how the filtering step does not remove the longest and most important eyelashes. Eyelashes are pictured as both 3D renders (left) and projection on images (right). Colors are individually consistent in each row.*

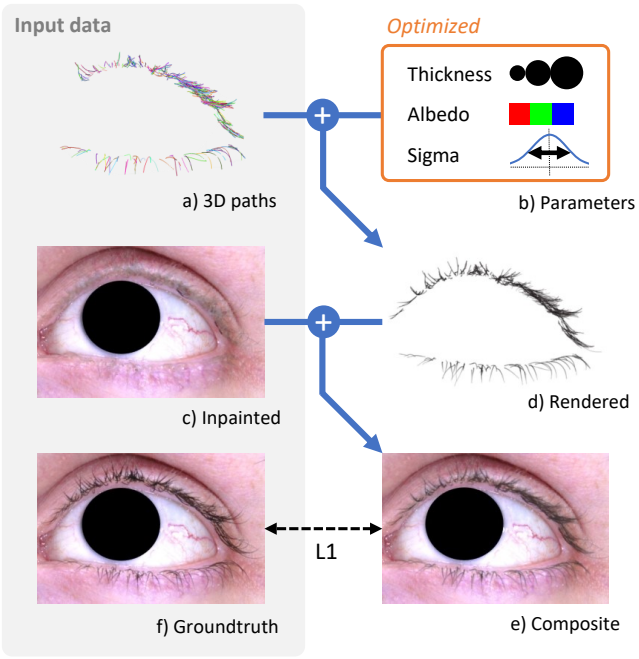

Figure 7: *Schema of the thickness and albedo estimation based on differentiable rendering with Pulsar [LZ21].*

Consequently, the segmentation maps generated by EyelashNet cannot serve as a reliable basis for estimating eyelash thickness. As shown in Figure 7, we start directly from the multiview images (c, f) and perform differentiable rendering (d) to optimize eyelash thickness and albedo (b). We use the reconstructed eyelashes (a) that we oversample to get a dense sequence of 3D points. Then, we associate a default radius of 0.02 mm to each of these points and a default albedo in RGB format (0.1, 0.1, 0.1). To render differentiably the predicted images, we use Pulsar [LZ21] as it is fast and well-suited for our one-dimensional geometry, the eyelashes being rendered as a sequence of spheres. The predicted images (d) are composited with the images with inpainted out eyelashes (c) and compared to the original ones (f) with L1 distance. Both the radius and albedo associated to each point are optimized in less than 50 iterations as depicted in Figure 14.

As for the implementation details, we initially optimize a Gaussian blur factor σ on each view since the eyelashes tend to be blurry due to camera depth of field. Secondly, the radius and albedo are not optimized *directly* for each sphere, but only for $n = 6$ control points per eyelash, and the intermediate radii and albedos are linearly interpolated which yields smoother results. Thirdly, since hair structures have strong specular components, we optimized a different albedo for each view and the final albedo is found to be the darker one. This makes it possible to successfully ignore the specular component that we did not estimate in this work.

4. Eyelash Modeling

Human eyelashes exhibit a growth cycle spanning from 1 to 3 months, with a lifespan of up to 9 months [TBC*09]. Remarkably, this means that our eyelashes undergo complete renewal on an annual or more frequent basis, while maintaining a consistent overall appearance. Building upon this intriguing phenomenon, we propose that the precise geometry of individual eyelashes holds relatively little significance in the context of human perception compared to their collective shape, represented by the statistical distribution of attributes along the eyelids. Our model relies on spatially dependent Gaussian distributions of the physical parameters that describe each individual eyelash. These distributions are governed by meta-parameters (mean and a notion of dispersion) that vary along the eyelids or along the eyelashes. To simplify their representation, we use equally spaced control points and interpolate between them.

Our eyelashes model relies on spatially-dependent distributions of the physical parameters of each individual eyelash. In contrast to Sacha *et al.* [SFWV06], we leverage real data to constrain our model to remain in the domain of plausible, anatomically realistic eyelashes. We also introduce the density and albedo parameters that greatly impact appearance. Another difference resides in the eyelash curvature representation. The authors used a three-point model interpolated with a cubic spline, while we employ a circular arc, thus making the curvature and length parameters independent.

4.1. Eyelash Model

Each synthetic eyelash is represented as a 3D circular arc, parameterized by its length, curvature, thickness, albedo, root position and root orientation (see Table 1). The root position is itself parameterized with UV coordinates spanning a predefined triangular mesh that also contains base orientation information at each vertex, represented by frames $[\mathbf{b}_x, \mathbf{b}_y, \mathbf{b}_z]$.

As depicted in the top left corner of Figure 8, u spans the contours of the eye, passing by the outer corner while v manages the distance that separates the root from the eyeball surface. Each eye-

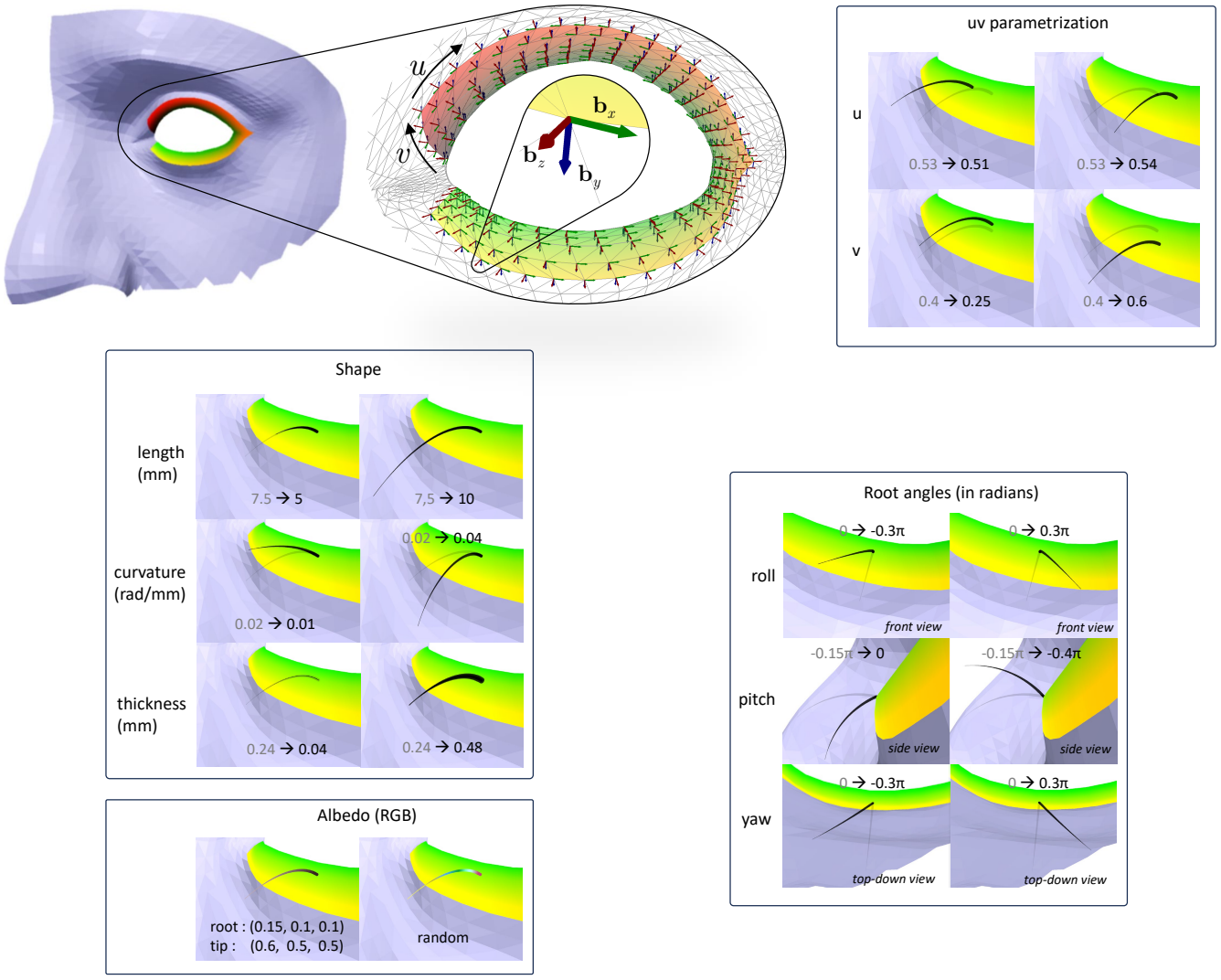

Figure 8: *Eyelash model presentation. For each parameter, the results of a value decrease and increase from a default value (in grey) are displayed.*

lash root orientation is expressed in the base orientation frames as a small rotation independent from the global pose. The base orientation is computed as follows : $\mathbf{b}_z$ is the direction from the eyeball center to the surface point, $\mathbf{b}_x$ is the direction associated with a small u decrease and $\mathbf{b}_y$ is the direction associated with a small v increase. Orthogonality is enforced with priority order $\mathbf{b}_z$, $\mathbf{b}_x$, $\mathbf{b}_y$. Because we use the eyeball center and the surface point to compute $\mathbf{b}_z$, this formulation adapts to any eye region morphology and pose. This makes it possible to easily transfer a set of eyelashes from one morphology to another and to move the eyelashes accordingly when the eye region is animated. Figure 8 illustrates the effect of each parameter on a single eyelash and Table 1 summarizes the eyelash model parameters.

4.2. Eyelashes Model

A set of eyelashes is represented by the statistical distributions of the parameters of each individual eyelash along the contours of the eye *i.e.* along u, assuming that all the distributions are Gaussian. For clarity, u is split into two parts u_u, u_l for upper and lower eyelids. We define the *eyelash density* as the density function along u_u or u_l scaled by the number of eyelashes on the corresponding eyelid, which makes it possible to combine the spatial distribution and the number of eyelashes in one profile curve.

Just like *eyelash density*, the other parameters of our synthetic eyelash set model are defined as profile curves, but with an additional measure of statistical dispersion. This means that curvature, length, v (*i.e.* distance to eyeball), root angles, thickness and albedo are defined by two profile curves representing their mean and standard deviation, respectively. Taking the dispersion into account en-

ables to control the fuzziness of the generated eyelashes which has great impact on the final appearance. There are specific cases for thickness and albedo parameters which are expressed with respect to the eyelash length instead of the eyelid path, but the methodology remains similar.

To express the profile curves in the discrete domain, we used a set of p control points in regular horizontal steps where the values in between are linearly interpolated. One of the parameters requires one profile curve, and ten parameters that require two profile curves. The total number of scalar parameters is therefore $1 \cdot p + 10 \cdot 2p = 21p$, $42p$ for both eyelids. In all our experiments, we used $p = 6$.

To synthesize a set of eyelashes from this model, we decompose the *eyelash density* back into a density function and a number of eyelashes. The u parameter of each eyelash is then randomly sampled according to the density function. By leveraging the statistical mean and dispersion of the other parameters and the u coordinate, we randomly sample them assuming a Gaussian distribution. The angle parameters (yaw, pitch, roll angles) follow a von Mises distribution, which is an approximation of the normal distribution wrapped on the unit circle. Their dispersion is represented as $\kappa^{-\frac{1}{2}}$, where κ is the von Mises concentration parameter. Table 2 summarizes the eyelashes model parameters.

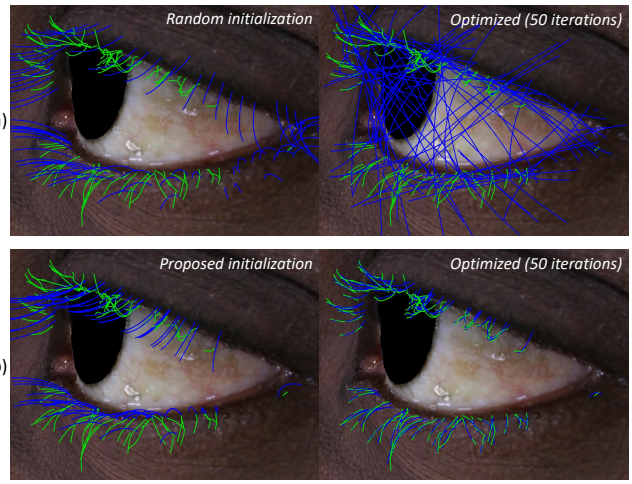

Figure 9: *Illustration of our eyelash parameter estimation using geometric fitting with random (a) and proposed (b) initialization. Reconstructed eyelashes appear in green and eyelash models are in blue.*

4.3. Parameter Estimation

By leveraging the 3D eyelashes of the 57 participants, we estimated the real world distribution of the eyelashes model parameters. We started on a microscopic scale by individually fitting the eyelash model to each reconstructed eyelash, then we computed the macroscopic parameters that describe all eyelashes at once.

Eyelash Parameter Estimation. First, the length, curvature, root angles and root position (see Table 1) are estimated for each reconstructed eyelash using a gradient descent optimization scheme (Figure 9). As an initialization step, we look for the UV parameterization of the nearest point on the skin to the reconstructed root, then we instantiate an individual eyelash model at this location that we optimize to fit the geometry of the reconstructed eyelash. The initialization step is mandatory to achieve convergence as shown in Figure 9. We use an optimization-based fitting in order to constrain the parameters to remain between plausible bounds. For instance, the root should rest on the predefined skin area. As an objective function, we use the Chamfer distance between the points of the eyelash model instance and those of the reconstructed eyelash. The Chamfer distance has the advantage of being robust regarding the gap between the root of the reconstructed eyelashes and the skin. The convergence of this geometric fitting is typically achieved in five iterations but we went up to 50 iterations in our experiments. We emphasize that the goal of this step is to estimate the parameters of our eyelash model using real data, rather than aiming for a perfect fit. The collected data is leveraged to provide a descriptive statistical analysis of the human eyelash shape, more information can be found in Appendix A.

Eyelash Set Parameter Estimation. Our eyelashes model relies on the spatial distribution of the eyelash model parameters (see Table 2). All the individual eyelash related parameters are represented as functions of the horizontal root position (*i.e.* the u parameter) with profile curves. There is an additional *eyelash density* parameter which informs about the distribution of the eyelash roots. To estimate *eyelash density*, we perform a Kernel Density Estimation (KDE) with a Gaussian kernel and bandwidth equal to 7.5% of the eyelid length. The p control points representing the associated profile curve are directly fitted to the KDE estimate.

The control points associated to the 10 other parameters are computed in a similar manner. Since the other parameters represent distributions, the profile curve of the distance to the mean is also computed. It must be noted that the angle parameters, *i.e.* the root angles, are represented as wrapped normal distributions approximated by von Mises distributions. To stay consistent with the other parameters, we use $\kappa^{-\frac{1}{2}}$ as a measure of the statistical dispersion.

Eyelash Set Parameters Calibration. The described parameter estimation is performed for each set of reconstructed eyelashes with the dedicated 3D reconstruction method detailed in Section 3. The resulting condensed eyelash information is leveraged to constrain the range of each parameter of our eyelashes model. In practice, the parameters are limited to a range of twice the standard deviation around the mean of all the estimated eyelashes parameters. This helps remain within the domain of realistic eyelashes while offering important modeling freedom.

5. Results

To validate our approach and highlight its potential applications, this section presents comparisons with two other reconstruction methods and shows different new use cases made possible thanks to our approach. We also provide insights on our pipeline implementation and running time.

Name	*Description*	*Estimation method*
Root position	Root parametrized location on predefined skin area (Figure 8)	Geometric fitting (Section 4.3)
Length	Eyelash root to tip distance	Geometric fitting (Section 4.3)
Curvature	Angle per unit distance along the eyelash	Geometric fitting (Section 4.3)
Root angles	Euler angles at the start of the eyelash from the base frame (Figure 8)	Geometric fitting (Section 4.3)
Thickness	Eyelash diameter	Differentiable rendering fitting (Section 3.6)
Albedo	Diffuse eyelash color	Differentiable rendering fitting (Section 3.6)

Table 1: *Summary of our Eyelash Model parameters*

Name	*Description*	*Distribution*	*Representation*	*Estimation method*
Density	Encodes the eyelashes repartition as the product of the number of eyelashes by the density function of their u parameter	-	Linear interpolation between uniformly spaced control points	Kernel Density Estimation then curve fitting
Length, curvature, thickness and albedo	Spatially distributed version of Eyelash Model's length, curvature, thickness and albedo	Gaussian	Linear interpolation between uniformly spaced control points for both mean μ and standard deviation σ	Curve fitting
Root angles	Spatially distributed version of Eyelash Model's root angles	Von Mises	Linear interpolation between uniformly spaced control points for both μ and standard deviation $\kappa^{-\frac{1}{2}}$	Curve fitting

Table 2: *Summary of our Eyelashes Model parameters*

5.1. Implementation and Performance

We implemented each block of our pipeline exclusively in Python. The libraries Numpy [HMvdW*20], Scipy [VGO*20], Numba [LPS15], Pytorch [PGM*19], Pytorch3D [RRN*20], OpenCV [Bra00], Matplotlib [Hun07], and Pyvista [SK19] were used for acceleration purposes, optimization procedures and visualization.

Our 3D eyelash reconstruction method takes ~13 min to run from end to end. Specifically, ~10 min for the 2D eyelash growing, ~1 min for the 3D segment matching, ~1 min for the 3D eyelash growing, and ~1 min for the thickness and albedo optimization which was performed using Adam optimizer [KB17] with a learning rate of 10^{-2}.

The shape parameters extraction method converges in less than 50 iterations (5 iterations already provide satisfactory results) that usually take ~4 s in total. The optimizer used is RMSprop with a learning rate of $2.5 \cdot 10^{-2}$. The eyelashes model parameters extraction procedure takes ~5 s. Sampling new eyelashes takes ~25 ms and the generation of the 3D geometry takes ~15 ms. Rendering a set of eyelashes takes ~150 ms. In our interactive application, the total update duration is ~500 ms.

All the experiments were conducted on a machine with an Intel(R) Xeon(R) Gold 3.40 GHz CPU, and a single NVIDIA RTX 2080 Ti GPU.

5.2. Eyelash Reconstruction

We show qualitative comparisons of our eyelash reconstruction method of Beeler *et al.* [BBN*12] and Nam *et al.* [NWKS19]. To carry out a fair comparison, we manually removed non-eyelashes hairs in the results of concurrent methods and excluded the thickness and albedo estimation from ours. Figure 10 shows the qualitative comparison with the approach of Beeler *et al.* on their 14 cameras multiview dataset. Our method successfully reconstructs a greater number of eyelashes and highly minimizes the scattering of reconstructed eyelashes into fragmented pieces, resulting in a more coherent and plausible appearance. Figure 11 shows the qualitative comparison with the approach of Nam *et al.* on the 12 cameras multiview dataset [KADM22]. The results of our method better follow the shapes of the eyelashes when Nam's *et al.* produce many false positives, some fragmented eyelashes and more noise in the global look of the eyelashes. In summary, our proposed method is the best in the context of eyelash modeling (Section 4) and statistical analysis (Appendix A).

To provide more insights into the robustness of our algorithm, we present results for challenging cases (Figure 12) and with fewer cameras (Figure 13). Challenging cases include very short eyelashes (a), light-colored eyelashes (b), low-contrast due to dark skin (c) and recessed eyelashes (d). Short eyelashes (a) are well reconstructed, as most of them have a good coverage by the projected overlay. The low-contrast case (c) results in a reasonable reconstruction with some missing eyelashes. Indeed, for three of the challenging cases (b, c and d) EyelashNet [XZZ*21] generates partially incomplete segmentation maps. especially for light-colored (b) and recessed (d) eyelashes. This leads to incomplete reconstruction. Figure 13 illustrates the impact of reducing the number of views on the reconstruction quality. It can be noted that two cameras are enough to output incomplete but accurate coverage. With four cameras, more eyelashes are reconstructed and with twelve cameras, our default setup, the reconstruction is almost exhaustive.

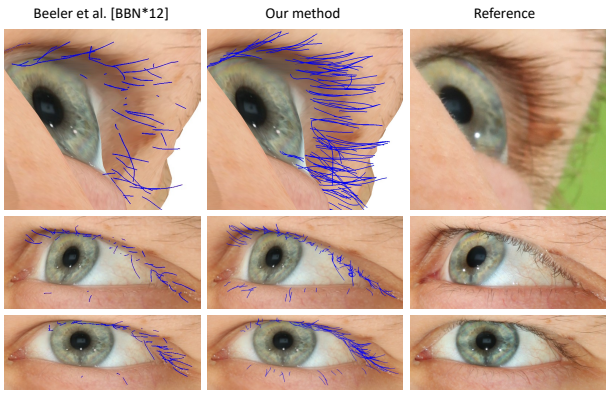

Figure 10: *Comparison of our reconstruction method and the method of Beeler* et al. *[BBN*12]. Our method produces denser and more high-fidelity results.*

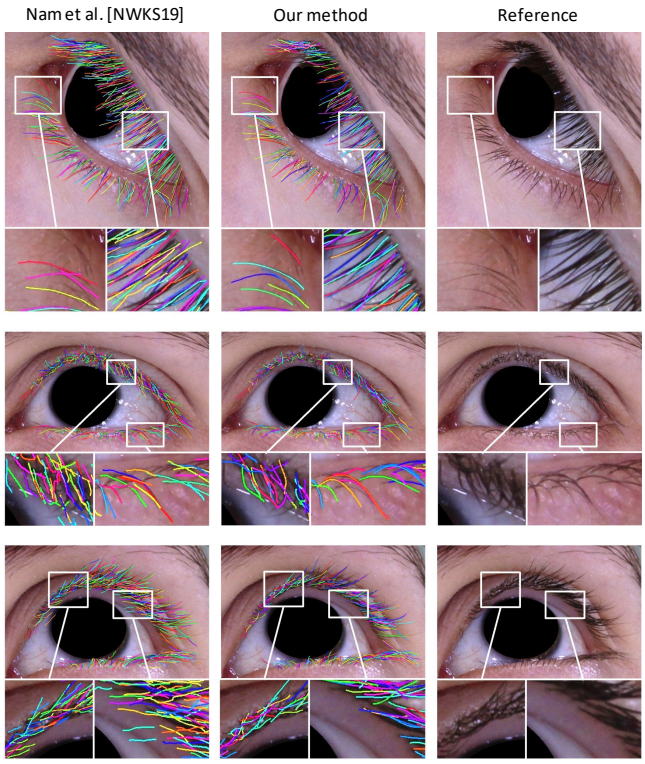

Figure 11: *Comparison of our reconstruction method and the method of Nam* et al. *[NWKS19]. Eyelashes are color coded to bring out the differences. Our method produces less false positives and better follow the eyelashes shapes.*

Figure 14 shows qualitative results of thickness and albedo estimation (Section 3.6) on three individuals (a, b and c). After initialization, the eyelashes appear too bold and dark (left). After 50 iterations (center), they look almost identical to the ones in the reference image (right), indicating an accurate fit.

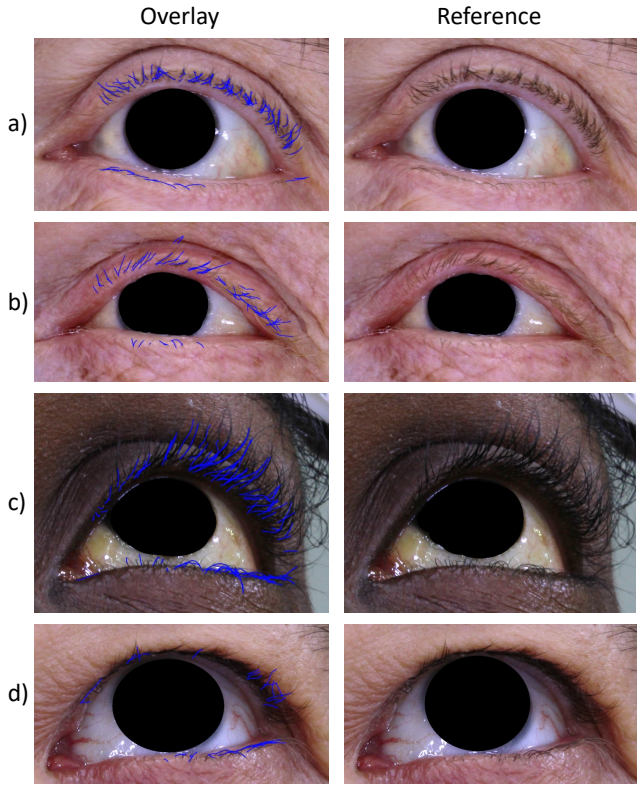

Figure 12: *Challenging reconstruction results with (a) very short eyelashes, (b) light-colored eyelashes, (c) low-contrast due to a dark skin, (d) recessed eyelashes occluded in most view angles.*

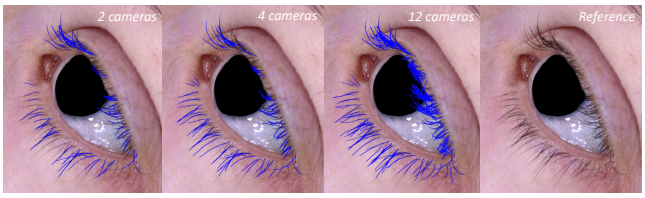

Figure 13: *Eyelash reconstruction results with two, four and twelve cameras.*

5.3. Model Validation

An interesting property of our eyelashes model is its independence from eye morphology. It allows easy eyelash swapping as demonstrated in Figure 15. The eyelashes of each subject are transferred to the morphology of each other subject. The reference images are shown in the diagonals. The appearance of each target eye is significantly modified depending on the source eyelashes being applied. It can be noted that the same eyelashes pattern is easily recognizable while being transferred onto a new target eye.

As our eyelashes model is parameterized by spatially varying statistical distributions, it describes an infinite number of eyelash arrangements for each set of parameters. However, samples from the same parameters should produce a very similar overall appearance. Figure 16 shows an example of eyelash resampling in two

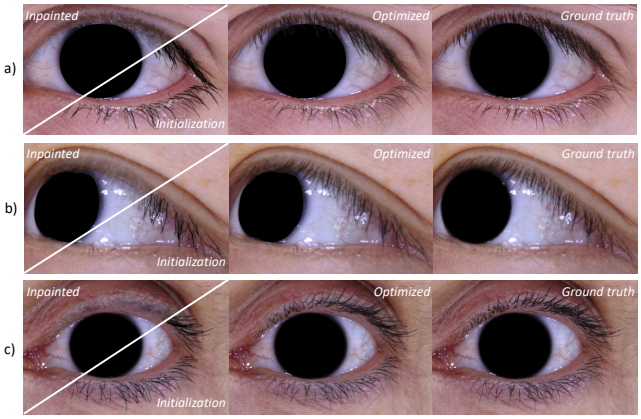

Figure 14: *Results of thickness and albedo optimization on three subjects (a, b, c). The first column shows the image with withdrawn (inpainted) eyelashes and the initialized synthetic eyelashes (initialization). The middle and right-hand columns correspond to the optimized result and target ground truth, respectively.*

subjects. The rendered resampled eyelashes follow the distributions of the eyelashes in the reference image which give them an arguably similar appearance. By swapping the parameters between the two subjects, we see that this property holds independently from the eye morphology, thus highlighting the stability of our model.

5.4. Semantic Editing

To validate the semantic editing capability of our model, we developed an intuitive and interactive application with a dedicated user interface illustrated in Figure 17. This application allows for a non-expert user to tune the semantic parameters of our model (a) and observe the effect at interactive rates (~500 ms) in both a Pulsar [LZ21] rendering window (b) and a 3D viewer (c). To guarantee that the visualization windows may be smoothly updated, we sampled standard normal distributions and standard von Mises distributions once, and mapped the samples dynamically onto the desired distributions.

Figure 18 shows four different semantic manipulations on two subjects from different viewpoints. First, a user drags the control points of the density profiles (a) to make the upper eyelid sparser and the lower eyelid denser. Then, the mean length of the eyelashes is modified (b), lower eyelashes are shortened while upper eyelashes are increasingly extended as they approach the outer corner of the eye. On another subject, the user decides to increase the curvature as well as the fuzziness with respect to the curvature (c) in the outer eye corner. Lastly, the roll angle (also called curl angle [SFWV06]) is modified (d) such that the eyelashes are directed the other way. These diverse manipulations produce the expected results on generated eyelashes, while keeping a realistic aspect thanks to the value ranges extracted from real data.

6. Discussion

When we propose an original eyelash modeling approach that enables new applications, our system comes with some limitations that should be addressed in future work. For both the reconstruction and the model, a registered mesh of the subject's eye is required. The authors of the original dataset [KADM22] relied on manual scan annotations to obtain them. However, we argue that state-of-the-art 2D/3D head alignment methods [LBB*17; BLB23; XQH*22] can alleviate this issue to enable full automation from input photographs.

The dedicated 3D eyelash reconstruction method allows the estimation of hair thickness and albedo. However, albedo makes little sense in the context of photo-realistic hair rendering due to the unique nature of hair that exhibits strong and unique specular components. In the original multi-view eye regions dataset, the light positions are unknown which limits the use of more appropriate light scattering models [MJC*03; CBTB15]. We limit this issue by estimating an albedo per view and setting the final albedo as the darkest across all views per point, but this leaves room for improvement.

In another setting, eyelash inpainting sometimes leaves unwanted artifacts. In columns (c) of Figure 15, it can be noted that the inpainted images contain floating residues of original eyelashes. Fine-tuning EyelashNet [XZZ*21] with the reconstructed data and additional synthetic data generated with the proposed model would probably lead to better segmentation predictions.

While impacting the appearance of an eye, eyelash clumping is not considered in our semantic model. The issue is visible in Figure 16 where the resampled eyelashes of subject (2) tend to clump together due to the replicated orientation distribution, but visibly not as much as in the reference image. This phenomenon can have various causes including natural oils, humidity, health conditions and other unknown factors. Incorporating clumping in our model offers an interesting research direction. It is currently handled as a post-processing step in our methodology.

7. Conclusion

We propose the first data-driven generative model of eyelashes based on semantic features. It has been obtained from real data using a novel 3D eyelash multi-view reconstruction method which outperforms existing ones for this specific task. Reconstructed data constitutes the first eyelashes dataset and will be made accessible for the research community. We also presented an original extraction process to estimate the semantic features of eyelashes from reconstructed ones. Extracted parameters were leveraged to calibrate our eyelashes model and to build a detailed descriptive statistics analysis of human eyelash shapes (Appendix A). Our eyelashes model successfully represents the overall appearance of a person's eyelashes while offering semantic control and guaranteeing the generation of plausible samples. Through different use cases such as eyelash transfer or semantic editing, we showed the power and strength of this new model. Our results demonstrated that the proposed model allows interactive, intuitive and realistic eyelash modeling for non-experts, thus enriching avatar creation and synthetic data generation pipelines.

8. Acknowledgments

We would like to thank Jules Saïdane for his precious work on manual annotation of our dataset, Derek Bradley (Disney Research) for

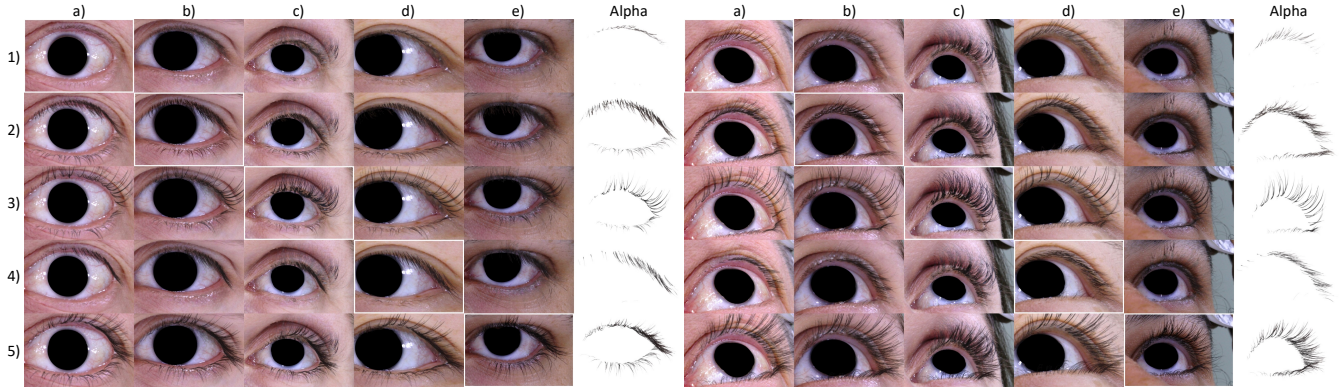

Figure 15: *Eyelash swapping with our model. The eyelashes of the subject of the i-th row are transferred to the subject of the j-th column. In the diagonal, the reference image is shown. The eyelashes without a background are also displayed in the rightmost column. The left part of the figure shows a frontal view and the right part shows a view from below.*

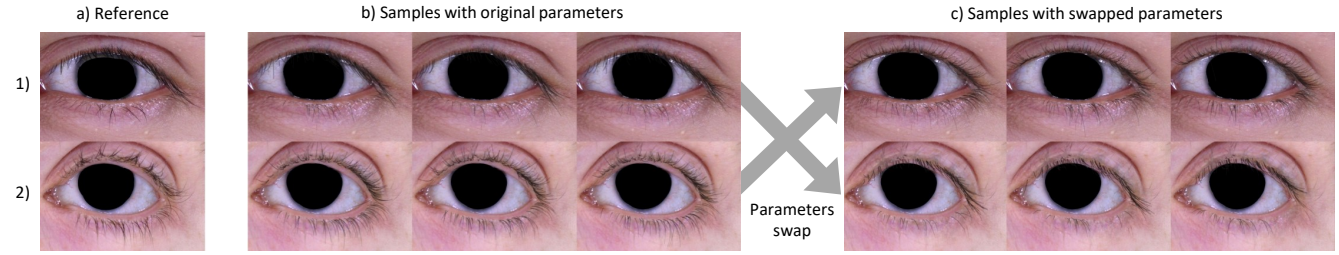

Figure 16: *Two reference eyes (a) are used to demonstrate how eyelash resampling preserves appearance. The original parameters are resampled three times to generate new eyelash arrangements which closely share the same overall appearance. Parameters are then swapped and eyelashes are sampled again three times (c) to show that this property remains on other target morphologies.*

providing a link to their dataset and Giljoo Nam (Meta) for running his LPMVS and strand generation algorithm on our dataset.

References

[AB18] AUMOND, SARAH and BITTON, ETTY. "The eyelash follicle features and anomalies: A review". *Journal of Optometry* 11 (July 2018). DOI: 10.1016/j.optom.2018.05.003 16.

[Ada21] ADAM, AIMEE. "Beauty is in the eye of the beautiful: Enhanced eyelashes increase perceived health and attractiveness." *Evolutionary Behavioral Sciences* 15.4 (Oct. 2021), 356–367. DOI: 10.1037/ebs0000192. URL: https://doi.org/10.1037%2Febs0000192 2.

[Aut23] AUTODESK. *Maya*. 2023. URL: https://%20autodesk.com/maya 2.

[BAC*06] BERTAILS, FLORENCE, AUDOLY, BASILE, CANI, MARIE-PAULE, et al. "Super-Helices for Predicting the Dynamics of Natural Hair". *ACM Transactions on Graphics* 25.3 (July 2006), 1180–1187. DOI: 10.1145/1141911.1142012 3.

[BBGB16] BÉRARD, PASCAL, BRADLEY, DEREK, GROSS, MARKUS, and BEELER, THABO. "Lightweight Eye Capture Using a Parametric Model". *ACM Transactions on Graphics* 35.4 (2016). ISSN: 0730-0301 1.

[BBGB19] BÉRARD, PASCAL, BRADLEY, DEREK, GROSS, MARKUS, and BEELER, THABO. "Practical Person-Specific Eye Rigging". *Comp. Graph. Forum* 38 (2019) 1.

[BBK*15] BERMANO, AMIT, BEELER, THABO, KOZLOV, YEARA, et al. "Detailed Spatio-Temporal Reconstruction of Eyelids". *ACM Trans. Graph.* 34.4 (2015). ISSN: 0730-0301 1.

[BBN*12] BEELER, THABO, BICKEL, BERND, NORIS, GIOACCHINO, et al. "Coupled 3D Reconstruction of Sparse Facial Hair and Skin". *ACM Transactions on Graphics* 31 (4 Aug. 2012), 117:1–117:10. DOI: 10.1145/2185520.2185613 1, 3–5, 9, 10.

[BBN*14] BÉRARD, PASCAL, BRADLEY, DEREK, NITTI, MAURIZIO, et al. "High-Quality Capture of Eyes". *ACM Transactions on Graphics* 33.6 (2014). ISSN: 0730-0301 1.

[BLB23] BOLKART, TIMO, LI, TIANYE, and BLACK, MICHAEL J. "Instant Multi-View Head Capture through Learnable Registration". *Proc. of Conference on Computer Vision and Pattern Recognition*. 2023, 768–779 11.

[Bra00] BRADSKI, G. "The OpenCV Library". *Dr. Dobb's Journal of Software Tools* (2000) 9.

[BV99] BLANZ, VOLKER and VETTER, THOMAS. "A Morphable Model for the Synthesis of 3D Faces". *Proc. of SIGGRAPH*. 1999, 187–194. ISBN: 0201485605 1.

[BWH*01] BARON-COHEN, SIMON, WHEELWRIGHT, SALLY J., HILL, J, et al. "The "Reading the Mind in the Eyes" Test revised version: a study with normal adults, and adults with Asperger syndrome or high-functioning autism." *Journal of child psychology and psychiatry, and allied disciplines* 42 2 (2001), 241–51 1.

[BWR*08] BERGOU, MIKLÓS, WARDETZKY, MAX, ROBINSON, STEPHEN, et al. "Discrete Elastic Rods". *ACM SIGGRAPH 2008 Papers*. SIGGRAPH '08. Los Angeles, California, 2008. DOI: 10.1145/1399504.1360662 3.

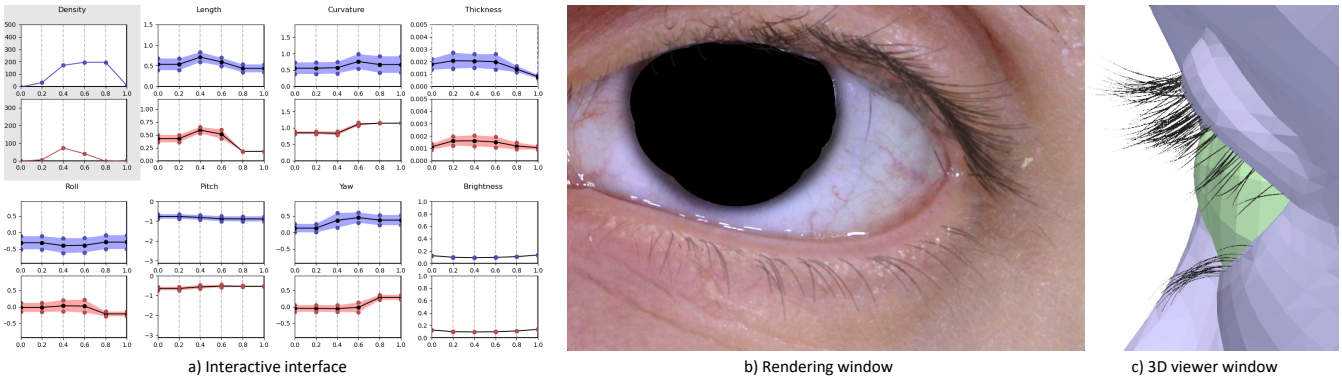

Figure 17: *The demonstrated 3D eyelash modeling interface. (a) A Matplotlib [Hun07] window displays the eyelashes model parameters as profile curves guided by control points for both mean and dispersion editing. The blue and red colors correspond to the upper eyelid and lower eyelid, respectively. Results are simultaneously displayed on two other windows (b) a Pulsar [LZ21] rendering window and (c) a 3D viewer powered by Pyvista [SK19].*

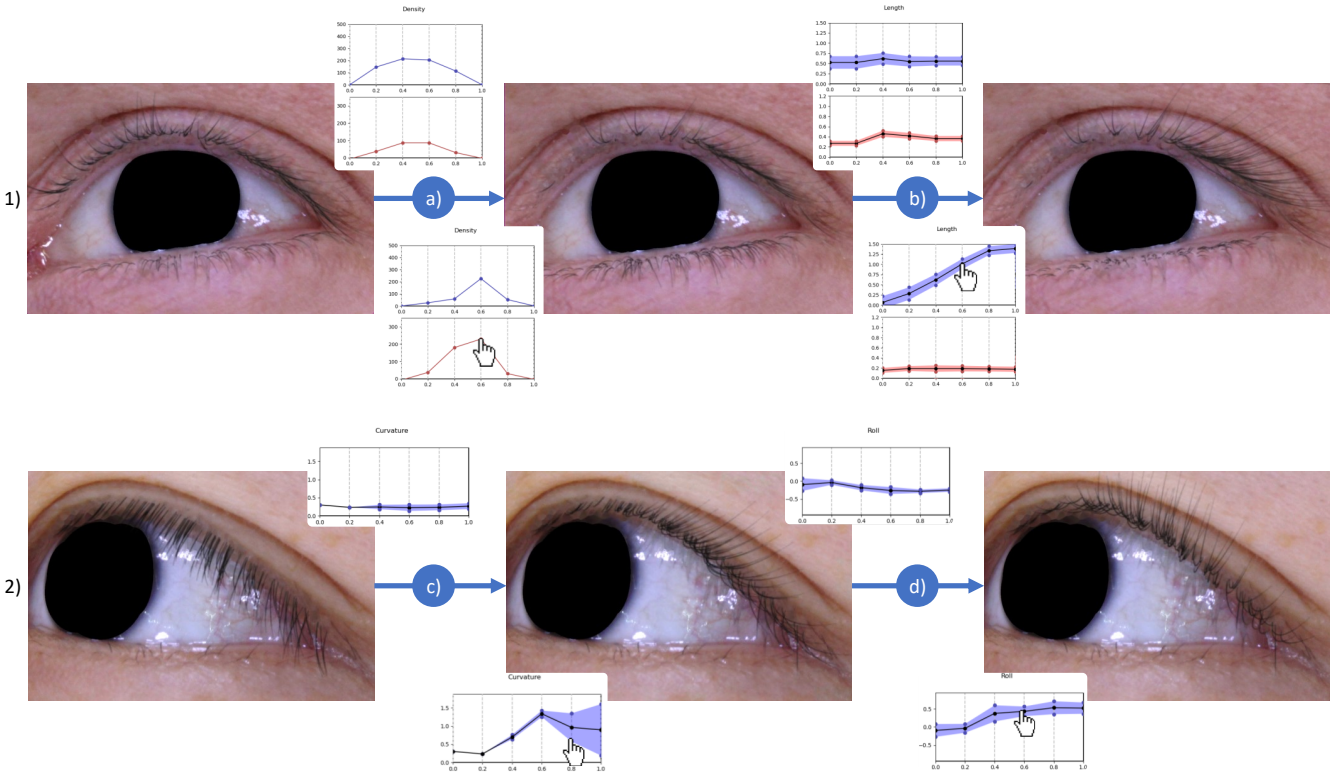

Figure 18: *Illustration of semantic eyelash editing. Four editing stages (a, b, c, d) are performed on two subjects displayed from different viewpoints. The blue and red colors correspond to the upper eyelid and lower eyelid parameters, respectively.*

[CBTB15] CHIANG, MATT JEN-YUAN, BITTERLI, BENEDIKT, TAPPAN, CHUCK, and BURLEY, BRENT. "A Practical and Controllable Hair and Fur Model for Production Path Tracing". *Proc. of ACM SIGGRAPH Talks*. 2015. DOI: 10.1145/2775280.2792559 11.

[Com20] COMMUNITY, MAKEHUMAN. *MakeHuman*. 2020. URL: http://www.makehumancommunity.org 2.

[CSW*16] CHAI, MENGLEI, SHAO, TIANJIA, WU, HONGZHI, et al. "AutoHair: Fully Automatic Hair Modeling from A Single Image". *ACM Transactions on Graphics* 35 (July 2016), 1–12. DOI: 10.1145/2897824.2925961 1.

[DPS18] DAI, HANG, PEARS, NICK, and SMITH, WILLIAM. "A data-augmented 3D morphable model of the ear". *Proc. of 13th IEEE International Conference on Automatic Face and Gesture Recognition*. 2018, 404–408. DOI: 10.1109/FG.2018.00065 1.

[Fou23] FOUNDATION, BLENDER. *Blender - a 3D modelling and rendering package*. 2023. URL: http://www.blender.org 2.

[Fyf12] FYFFE, GRAHAM. "High fidelity facial hair capture". *Proc. of ACM SIGGRAPH Talks*. 2012 3.

[Gam23] GAMES, EPIC. *MetaHuman Creator*. 2023. URL: https://www.unrealengine.com/metahuman 2.

[GTZN21] GAFNI, GUY, THIES, JUSTUS, ZOLLHÖFER, MICHAEL, and NIESSNER, MATTHIAS. "Dynamic Neural Radiance Fields for Monocular 4D Facial Avatar Reconstruction". *Proc. of the IEEE/CVF Conference on Computer Vision and Pattern Recognition*. June 2021, 8649–8658 1.

[HML*14] HU, LIWEN, MA, CHONGYANG, LUO, LINJIE, et al. "Capturing Braided Hairstyles". *ACM Transactions on Graphics* 33.6 (2014), 225:1–225:9 2.

[HMvdW*20] HARRIS, CHARLES R., MILLMAN, K. JARROD, van der WALT, STÉFAN J., et al. "Array programming with NumPy". *Nature* 585.7825 (Sept. 2020), 357–362. DOI: 10.1038/s41586-020-2649-2 9.

[Hun07] HUNTER, J. D. "Matplotlib: A 2D graphics environment". *Computing in Science & Engineering* 9.3 (2007), 90–95. DOI: 10.1109/MCSE.2007.55 9, 13.

[JMM09] JAKOB, WENZEL, MOON, JONATHAN T., and MARSCHNER, STEVE. "Capturing Hair Assemblies Fiber by Fiber". *ACM Transactions on Graphics* 28.5 (Dec. 2009), 164:1–164:9. DOI: 10.1145/1618452.1618510 2.

[KADM22] KERBIRIOU, GLENN, AVRIL, QUENTIN, DANIEAU, FABIEN, and MARCHAL, MAUD. "Detailed Eye Region Capture and Animation". *Computer Graphics Forum* (2022). ISSN: 1467-8659. DOI: 10.1111/cgf.14642 1, 4, 9, 11.

[KB17] KINGMA, DIEDERIK P. and BA, JIMMY. *Adam: A Method for Stochastic Optimization*. 2017. arXiv: 1412.6980 [cs.LG] 9.

[KMI*15] KIKUCHI, MAMORU, MATSUDA, KEN, ISHIHARA, YASUHIRO, et al. "A study of normal eyelashes in Japanese individuals". 2015. URL: https://api.semanticscholar.org/CorpusID:53603063 2, 15, 16.

[KPKR17] KARCZMAREK, PAWEŁ, PEDRYCZ, WITOLD, KIERSZTYN, ADAM, and RUTKA, PRZEMYSŁAW. "A study in facial features saliency in face recognition: an analytic hierarchy process approach". *Soft Computing* 21 (Dec. 2017) 1.

[LBB*17] LI, TIANYE, BOLKART, TIMO, BLACK, MICHAEL. J., et al. "Learning a model of facial shape and expression from 4D scans". *ACM Transactions on Graphics* 36.6 (2017), 194:1–194:17. DOI: https://doi.org/10.1145/3130800.3130813 1, 11.

[LHWD17] LEGENDRE, CHLOE, HYUNH, LOC, WANG, SHANHE, and DEBEVEC, PAUL. "Modeling vellus facial hair from asperity scattering silhouettes". July 2017, 1–2. ISBN: 978-1-4503-5008-2. DOI: 10.1145/3084363.3085057 1, 3.

[LJZ*23] LI, CHENGHONG, JIN, LEYANG, ZHENG, YUJIAN, et al. *EMS: 3D Eyebrow Modeling from Single-view Images*. 2023. arXiv: 2309.12787 [cs.CV] 1, 3.

[LLCL19] LIU, SHICHEN, LI, TIANYE, CHEN, WEIKAI, and LI, HAO. "Soft Rasterizer: A Differentiable Renderer for Image-based 3D Reasoning". *Proc. of the IEEE International Conference on Computer Vision*. Oct. 2019 3.

[LLP*12] LUO, LINJIE, LI, HAO, PARIS, S., et al. "Multi-view hair capture using orientation fields". *Proc. of IEEE Conference on Computer Vision and Pattern Recognition*. June 2012, 1490–1497. DOI: 10.1109/CVPR.2012.6247838 2.

[LLR13] LUO, LINJIE, LI, HAO, and RUSINKIEWICZ, SZYMON. *Structure-Aware Hair Capture*. New York, NY, USA, July 2013. DOI: 10.1145/2461912.2462026 2.

[LPS15] LAM, SIU KWAN, PITROU, ANTOINE, and SEIBERT, STANLEY. "Numba: A LLVM-Based Python JIT Compiler". *Proc. of the ACM Second Workshop on the LLVM Compiler Infrastructure in HPC*. 2015. DOI: 10.1145/2833157.2833162 9.

[LWZ12] LAY HERRERA, TOMAS, WEBER, ANDREAS, and ZINKE, ARNO. "Lighting Hair From The Inside: A Thermal Approach To Hair Reconstruction". *ACM Transactions on Graphics* 31 (Dec. 2012) 2.

[LZ21] LASSNER, CHRISTOPH and ZOLLHOFER, MICHAEL. "Pulsar: Efficient Sphere-Based Neural Rendering". *Proceedings of the IEEE/CVF Conference on Computer Vision and Pattern Recognition (CVPR)*. June 2021, 1440–1449 6, 11, 13.

[LZWV10] LAY HERRERA, TOMAS, ZINKE, ARNO, WEBER, ANDREAS, and VETTER, THOMAS. "Toward image-based facial hair modeling". May 2010, 93. ISBN: 9781450305587. DOI: 10.1145/1925059.1925077 3.

[LZX*21] LIU, YILONG, ZHENG, CHENGWEI, XU, FENG, et al. "Data-Driven 3D Neck Modeling and Animation". *IEEE Transactions on Visualization and Computer Graphics* 27.7 (2021), 3226–3237. DOI: 10.1109/TVCG.2020.2967036 1.

[Max23a] MAXON. *Cinema4D*. 2023. URL: https://www.maxon.net/cinema-4d 2.

[Max23b] MAXON. *ZBrush*. 2023. URL: https://www.maxon.net/zbrush 2.

[MJC*03] MARSCHNER, STEPHEN R., JENSEN, HENRIK WANN, CAMMARANO, MIKE, et al. "Light Scattering from Human Hair Fibers". *ACM Transactions on Graphics* 22.3 (July 2003), 780–791. DOI: 10.1145/882262.882345 11.

[MSN*21] MCGUIRE, MORGAN, SUN, TIANCHENG, NAM, GILJOO, et al. "Human Hair Inverse Rendering using Multi-View Photometric data". *Proc. of Eurographics Symposium on Rendering*. 2021. URL: https://api.semanticscholar.org/CorpusID:235681666 2.

[NCRP16] NEOG, DEBANGA R., CARDOSO, JOÃO L., RANJAN, ANURAG, and PAI, DINESH K. "Interactive Gaze Driven Animation of the Eye Region". *Proc. of the Int. Conf. on Web3D Technology*. 2016, 51–59 1.

[NKK*06] NA, J.I., KWON, O.S., KIM, B.J., et al. "Ethnic characteristics of eyelashes: a comparative analysis in Asian and Caucasian females". *British Journal of Dermatology* 155.6 (Dec. 2006), 1170–1176 2, 16.

[NWKS19] NAM, GILJOO, WU, CHENGLEI, KIM, MIN H., and SHEIKH, YASER. "Strand-Accurate Multi-View Hair Capture". *Proc. of IEEE Conf. Computer Vision and Pattern Recognition*. June 2019 1–3, 9, 10.

[PBS04] PARIS, SYLVAIN, BRICEÑO, HECTOR M., and SILLION, FRANÇOIS X. "Capture of Hair Geometry from Multiple Images". *ACM Transactions on Graphics* 23.3 (Aug. 2004), 712–719. DOI: 10.1145/1015706.1015784 2.

[PCK*08] PARIS, SYLVAIN, CHANG, WILL, KOZHUSHNYAN, OLEG I., et al. "Hair Photobooth: Geometric and Photometric Acquisition of Real Hairstyles". *ACM Transactions on Graphics* 27.3 (Aug. 2008), 1–9. DOI: 10.1145/1360612.1360629 2.

[PGM*19] PASZKE, ADAM, GROSS, SAM, MASSA, FRANCISCO, et al. "PyTorch: An Imperative Style, High-Performance Deep Learning Library". *Proc. of the 33rd International Conference on Neural Information Processing Systems*. 2019 9.

[PMTZ22] PLOUMPIS, STYLIANOS, MOSCHOGLOU, STYLIANOS, TRIANTAFYLLOU, VASILEIOS, and ZAFEIRIOU, STEFANOS. "3D human tongue reconstruction from single" in-the-wild" images". *Proc. of the IEEE/CVF Conference on Computer Vision and Pattern Recognition*. 2022, 2771–2780 1.

[Rea22] REALLUSION. *Character Creator 4*. 2022. URL: https://www.reallusion.com/character-creator/ 2.

[RMLA19] ROTGER, GEMMA, MORENO-NOGUER, FRANCESC, LUMBRERAS, FELIPE, and AGUDO, ANTONIO. "Single View Facial Hair 3D Reconstruction". *Proc. of Iberian Conference on Pattern Recognition and Image Analysis*. 2019. URL: https://api.semanticscholar.org/CorpusID:174794044 3.

[RRN*20] RAVI, NIKHILA, REIZENSTEIN, JEREMY, NOVOTNY, DAVID, et al. "Accelerating 3D Deep Learning with PyTorch3D". *arXiv:2007.08501* (2020) 9.

[RSW*22] ROSU, RADU ALEXANDRU, SAITO, SHUNSUKE, WANG, ZIYAN, et al. "Neural Strands: Learning Hair Geometry and Appearance from Multi-view Images". *Proc. of European Conference on Computer Vision*. July 2022 3.

[RWX17] REN, YUN, WANG, ZULIN, and XU, MAI. "Learning-Based Saliency Detection of Face Images". *IEEE Access* 5 (2017), 6502–6514 1.

[SCD*23] SKLYAROVA, VANESSA, CHELISHEV, JENYA, DOGARU, ANDREEA, et al. "Neural Haircut: Prior-Guided Strand-Based Hair Reconstruction". *Proc. of IEEE International Conference on Computer Vision*. 2023 3.

[SFF*18] SHAIEK, AYET, FLAMENT, FRÉDÉRIC, FRANÇOIS, GHISLAIN, et al. "Morphological criteria of feminine upper eyelashes, quantified by a new semi-automatized image analysis: Application to the objective assessment of mascaras." *Skin Research and Technology* 24 (2018), 135–144. URL: https://api.semanticscholar.org/CorpusID:41967850 2, 16.

[SFWV06] SACHA, JAREK, FABULA, ANGELA, WYATT, PETER, and VICKERY, SARAH. "Simulating Realistic Eyelash Looks". *Proc. of ACM SIGGRAPH Research Posters*. 2006, 29–es. DOI: 10.1145/1179622.1179654 3, 6, 11.

[SK19] SULLIVAN, C. BANE and KASZYNSKI, ALEXANDER. "PyVista: 3D plotting and mesh analysis through a streamlined interface for the Visualization Toolkit (VTK)". *Journal of Open Source Software* 4.37 (May 2019), 1450. DOI: 10.21105/joss.01450 9, 13.

[Sof23] SOFTWARE, SIDE EFFECTS. *Houdini*. 2023. URL: https://www.sidefx.com/products/houdini/ 2.

[SSW*23] SHEN, YUEFAN, SAITO, SHUNSUKE, WANG, ZIYAN, et al. "CT2Hair: High-Fidelity 3D Hair Modeling Using Computed Tomography". *ACM Transactions on Graphics* 42.4 (July 2023). DOI: 10.1145/3592106 2.

[SWW*20] SCHWARTZ, GABRIEL, WEI, SHIH-EN, WANG, TENIA, et al. "The Eyes Have It: An Integrated Eye and Face Model for Photorealistic Facial Animation". *ACM Transactions on Graphics* 39.4 (2020) 1.

[TBC*09] THIBAUT, SEBASTIEN, BECKER, E, CAISEY, LAURENCE, et al. "Human eyelash characterization". *The British journal of dermatology* 162 (Sept. 2009), 304–10. DOI: 10.1111/j.1365-2133.2009.09487.x 6.

[TIIW18] TOHMYOH, HIRONORI, ISHIHARA, MITSUHARU, IKUTA, KAORI, and WATANABE, TOMOKO. "On the correlation between the curvature of the human eyelash and its geometrical features". *Acta Biomaterialia* 76 (2018), 108–115. DOI: https://doi.org/10.1016/j.actbio.2018.07.005 2.

[VGO*20] VIRTANEN, PAULI, GOMMERS, RALF, OLIPHANT, TRAVIS E., et al. "SciPy 1.0: Fundamental Algorithms for Scientific Computing in Python". *Nature Methods* 17 (2020), 261–272. DOI: 10.1038/s41592-019-0686-2 9.

[VPB*18] VELINOV, ZDRAVKO, PAPAS, MARIOS, BRADLEY, DEREK, et al. "Appearance Capture and Modeling of Human Teeth". *ACM Transactions on Graphics* 37.6 (Dec. 2018). DOI: 10.1145/3272127.3275098 1.

[WBG*16] WU, C., BRADLEY, D., GARRIDO, P., et al. "Model-Based Teeth Reconstruction". *ACM Transactions on Graphics* 35.6 (2016) 1.

[WBH*21] WOOD, ERROLL, BALTRUŠAITIS, TADAS, HEWITT, CHARLIE, et al. "Fake It Till You Make It: Face analysis in the wild using synthetic data alone". *Proc. of International Conference on Computer Vision*. 2021 2.

[WBM*16a] WOOD, ERROLL, BALTRUŠAITIS, TADAS, MORENCY, LOUIS-PHILIPPE, et al. "A 3D Morphable Eye Region Model for Gaze Estimation". *Proc. of ECCV*. 2016, 297–313 1.

[WBM*16b] WOOD, ERROLL, BALTRUŠAITIS, TADAS, MORENCY, LOUIS-PHILIPPE, et al. "Learning an Appearance-Based Gaze Estimator from One Million Synthesised Images". *Proc. of ACM Symp. on Eye Tracking Research and Applications*. 2016, 131–138 2.

[WNS*22] WANG, ZIYAN, NAM, GILJOO, STUYCK, TUUR, et al. "NeuWigs: A Neural Dynamic Model for Volumetric Hair Capture and Animation". *Proc. of IEEE/CVF Conference on Computer Vision and Pattern Recognition*. 2022 1–3.

[WOQS05] WEI, YICHEN, OFEK, EYAL, QUAN, LONG, and SHUM, HEUNG-YEUNG. "Modeling hair from multiple views". *ACM Transactions on Graphics* 24 (July 2005), 816–820. DOI: 10.1145/1073204.1073267 2.

[WZC*22] WINBERG, SEBASTIAN, ZOSS, GASPARD, CHANDRAN, PRASHANTH, et al. "Facial Hair Tracking for High Fidelity Performance Capture". *ACM Transactions on Graphics* 41.4 (July 2022). DOI: 10.1145/3528223.3530116 3.

[XQH*22] XIA, JIAHAO, QU, WEIWEI, HUANG, WEN-FONG, et al. "Sparse Local Patch Transformer for Robust Face Alignment and Landmarks Inherent Relation Learning". *Proc. of IEEE/CVF Conference on Computer Vision and Pattern Recognition*. 2022, 4042–4051. URL: https://api.semanticscholar.org/CorpusID:247447671 11.

[XZZ*21] XIAO, QINJIE, ZHANG, HANYUAN, ZHANG, ZHAORUI, et al. "EyelashNet: A Dataset and a Baseline Method for Eyelash Matting". *ACM Transactions on Graphics* 40.6 (Dec. 2021). DOI: 10.1145/3478513.3480540 2, 4, 9, 11.

[YMS*19] YANG, WENWU, MARSHAK, NATHAN, SÝKORA, DANIEL, et al. "Building anatomically realistic jaw kinematics model from data". *The Visual Computer* 35 (June 2019). DOI: 10.1007/s00371-019-01677-8 1.

[ZHX*18] ZHOU, YI, HU, LIWEN, XING, JUN, et al. "HairNet: Single-View Hair Reconstruction using Convolutional Neural Networks". *Proc. of ECCV*. June 2018 1.

Appendix A: Descriptive Human Eyelash Shape Analysis

We leveraged the 3D eyelash data collected using our novel 3D reconstruction approach (Section 3) to provide a descriptive analysis of human eyelash properties. Results are shown in Figure 19 where we plotted the eyelash data distributions on the respective eyelids. For each plot, the blue and red colors indicate the upper eyelid and lower eyelid, respectively. The relative root position (horizontal axis) represents the geodesic distance to the inner eye corner along the implantation area.

Plots a and d illustrate the probability density function that has been estimated using KDE and its product with the number of observed eyelashes, respectively. To enhance readability, data from the lower eyelid has been reflected w.r.t. the horizontal axis. The mean of each curve is overlaid at full opacity to highlight the general trend. These plots indicate that the upper eyelashes are more uniformly distributed than the lower ones which are concentrated towards the middle (a). Similar to existing research [KMI*15], we found that significantly more eyelashes grow on the upper eyelid than on the lower eyelid (d).

All the other plots show the global distributions of eyelash model parameters along the eyelids. Again blue and red colors are respectively associated to upper and lower eyelids. Each point represents an eyelash, and is color-coded to indicate the person to whom it belongs. The mean curve at full opacity is obtained with spline fitting trough the scattered points. The dispersion range at low opacity shows the mean standard deviation and is computed by fitting a spline to the squared centered data and taking its square root. We observe that upper eyelashes are slightly longer that lower eyelashes independently of the horizontal location (b, e) which coin-

cides with available literature [KMI*15; AB18]. Another interesting observation is that the length of the eyelashes seems to correlate with their density (d). More precisely, the longest eyelashes on average are located on the outer side of the upper eyelid (b) and in the middle of the lower eyelid (e). The lower eyelashes are more curved than the upper eyelashes, reaching up to a factor of two in the outer regions of the eyelids (c, f). The color-coding highlights extreme eyelash shapes distant from the mean. In fact, the blue dots observable at the top of plots b and e belong to the subject that appears in Figures 1, 2, 3, 4 and 15.

Global eyelash orientation data is also described in this appendix. The roll (g, j), pitch (h, k) and yaw (i, l) angles (also called curl, lift and siding angles) are plotted in the same manner as length and curvature. The roll angle shows important variance on the upper eyelid (g) but does not vary much spatially, neither does it on the lower eyelids (j). The pitch (h) and yaw (i) angles of upper eyelashes vary a little more spatially. On the outer eyelid, they fall more downwards (low pitch) and are oriented towards the outer corner (great yaw). On the lower eyelids, no particular pattern stands out for pitch and yaw angles.

In summary, we leverage our high-quality eyelash data (Section 3) and shape parameter estimation method (Section 4.3) to provide new insights on human eyelash shapes. For the first time, global statistics of human eyelash distributions and shape parameters are examined continuously along the eyelids, rather than using discrete intervals [SFF*18; NKK*06].

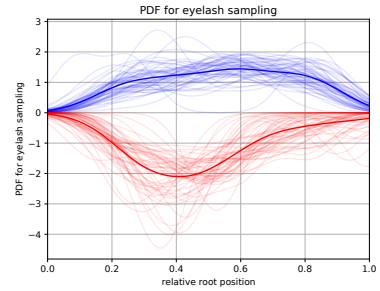

(a) *Eyelash probability density functions.*

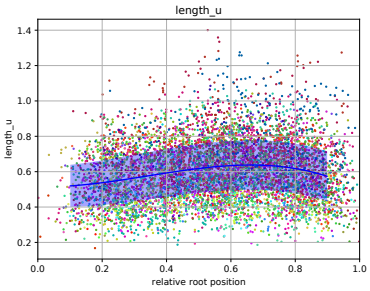

(b) *Global eyelash length distribution on the upper eyelid.*

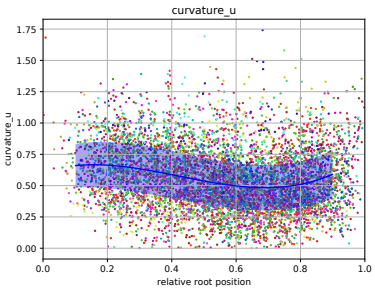

(c) *Global eyelash curvature distribution on the upper eyelid.*

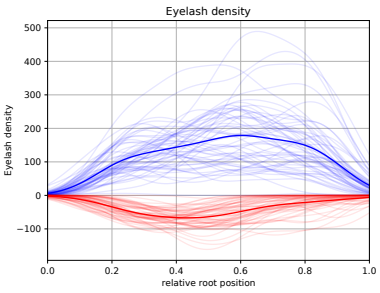

(d) *Eyelash densities.*

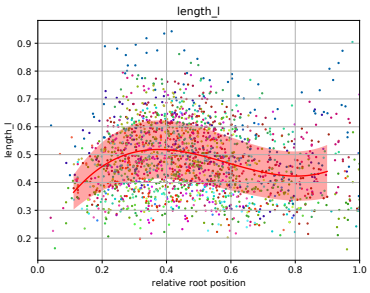

(e) *Global eyelash length distribution on the lower eyelid.*

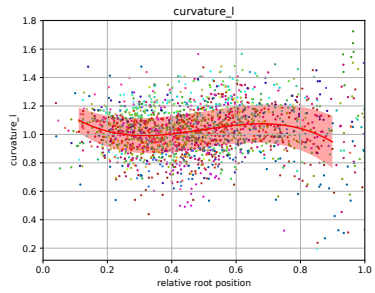

(f) *Global eyelash curvature distribution on the lower eyelid.*

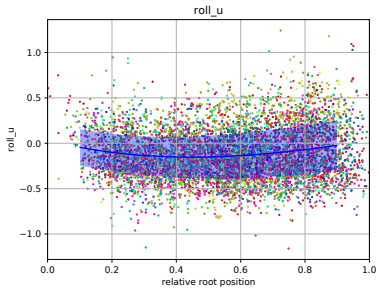

(g) *Global eyelash roll angle distribution on the upper eyelid.*

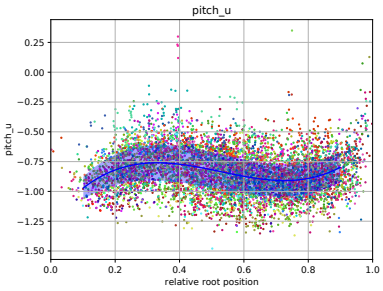

(h) *Global eyelash pitch angle distribution on the upper eyelid.*

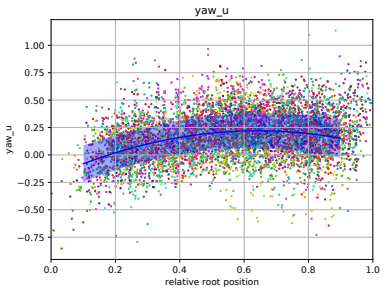

(i) *Global eyelash yaw angle distribution on the upper eyelid.*

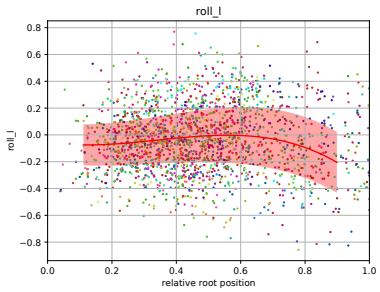

(j) *Global eyelash roll angle distribution on the lower eyelid.*

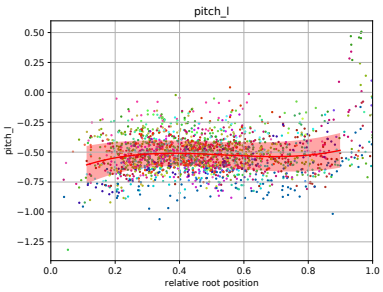

(k) *Global eyelash pitch angle distribution on the lower eyelid.*

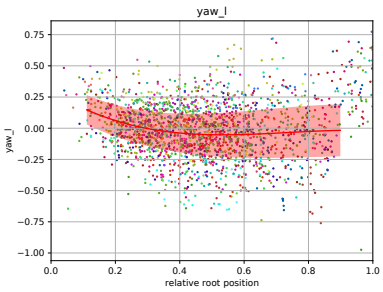

(l) *Global eyelash yaw angle distribution on the lower eyelid.*

Figure 19: *Global distributions of eyelash data along the eyelids in our dataset. The blue color represents upper eyelid data and the red color lower eyelid data. Plots a and d show the eyelash presence probability density functions and their product with the number of eyelashes on the eyelid, respectively. All the other plots describe the distribution of eyelash model parameters w.r.t. the eyelid paths. Each dot corresponds to an eyelash, and is color-coded to indicate the subject to whom it belongs.*